Inorganic Chemistry

Article

pubs.acs.org/IC

Selection for a Single Self-Assembled Macrocycle from a Hybrid Metal–Ligand Hydrogen-Bonded (MLHB) Ligand Subunit

Samantha K. Sommer, Ernst A. Henle, Lev N. Zakharov, and Michael D. Pluth*

Department of Chemistry and Biochemistry, Materials Science Institute, 1253 University of Oregon, Eugene, Oregon 97403, United States

Supporting Information

ABSTRACT: To expand the interface between self-assembled metal–ligand and hydrogen-bonded architectures, here we report the preparation, self-assembly, and metal–ligand binding of a pyridyl quinolone ligand (5-PYQ). The 5-PYQ ligand self-associates through quinolone hydrogen bonding, and it binds to metal centers through the pyridine ligand component. As a first step toward investigating more-complex hybrid metal–ligand hydrogen-bonded (MLHB) architectures, we report investigations of 5-PYQ with *mono-* and *bis*-platinated anthracene precursors. These results demonstrate that the 5-PYQ ligand maintains hydrogen bonding interactions while binding to square-planar platinum centers, but that generation of coordination compounds with closed topology erodes the hydrogen bonding fidelity to favor ambidentate coordination modes of the 5-PYQ ligand.

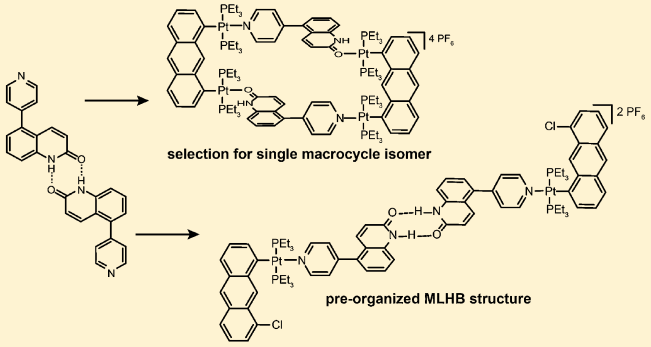

INTRODUCTION

Contrasting the established strategies for accessing purely hydrogen-bonded or metal–ligand-derived supramolecular architectures, the emerging area of self-assembly utilizing both hydrogen bonds and metal–ligand interactions in the same architecture has yet to establish well-defined, rational design strategies for selecting one discrete structure over other possible products. For example, a recent report demonstrated the formation of hybrid metal–ligand hydrogen-bonded (MLHB) triangles and squares from 2-ureido-4-[1*H*]-pyrimidinone and *cis*-substituted square planar Pd(II) components, but selective formation of a single discrete structure in solution was problematic.[1] Similarly, the potential to form oligomeric or polymeric self-assembled products over their closed hybrid MLHB counterparts, or the possibility of linkage isomer formation because of the ability of the hydrogen-bond acceptors to also act as ligands for metal coordination, also complicates the self-assembly of metal precursors with ligand subunits containing both metal-binding and hydrogen-bonding moieties. For example, the assembly of dinuclear organoplatinum(II) complexes with nicotinic acid afforded hybrid cyclic structures in solution; however, hybrid polymeric corrugated chains were present in the solid state, highlighting the challenges of engineering architectures with consistent solution and solid-state structures.[2] These, as well as other challenges including the limited number of fully characterized systems, constitute major limiting factors in developing rational design strategies to access closed hybrid MLHB assemblies.[1−13] Expansion of well-defined, discrete, characterized structures in this chemical space is warranted to develop well-defined assembly strategies for MLHB architectures and access the diverse landscape and full potential of these hybrid MLHB systems.

Toward the goal of generating discrete MLHB assemblies, we recently reported the design and preparation of a quinolone-based phosphine ligand **7-DPQ**, which we demonstrated assembles into a discrete hybrid MLHB structure with closed topology in the presence of a piano-stool rhodium metal precursor.[13] These results prompted us to explore the limits of self-assembly with similar quinolone ligands by modulating the metal-binding component of **7-DPQ** from a phosphine to a pyridine, thus providing access to different metal tectons and coordination directionality (see Scheme 1). Furthermore, the pendant pyridyl group should provide access to a diverse library of architectures, based on previous work with pyridine-containing ligands for metal–ligand self-assembly, particularly

Scheme 1. Comparison of the Structures of the Hybrid Subunits 7-DPQ and 5-PYQ

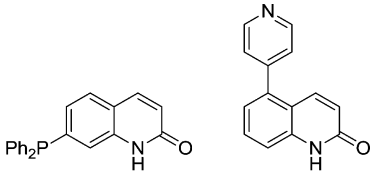

Received: April 15, 2015
Published: July 6, 2015

DOI: 10.1021/acs.inorgchem.5b00857
Inorg. Chem. 2015, 54, 6910–6916

when assembled with square planar platinum metal components.[14−17] As a first step toward investigating more complex architectures based on pyridine-containing MLHB ligands, we report here investigations of **5-PYQ** with *mono-* and *bis*-platinated anthracene precursors[18−21] to determine whether hybrid MLHB ligands provide selective access to discrete closed structures over potential oligomeric or polymeric assembly motifs. Many different assembly motifs are possible upon assembly of an ambidentate hybrid subunit, such as **5-PYQ**, with a bidentate metal acceptor. Possible final structures include hybrid polymers, metal−ligand complexes, symmetrical and asymmetrical macrocyclic isomers, hybrid closed MLHB macrocycles, or a mixture of these structures (see Scheme 2).

Scheme 2. Combination of Ambidentate Hybrid MLHB Ligand Subunit and Bidentate Metal Acceptor Can Lead to a Large Number of Possible Products, Hybrid Polymers, Metal−Ligand Complex, Macrocyclic Isomers, Hybrid Closed MLHB Macrocycle, or a Mixture of Products[a]

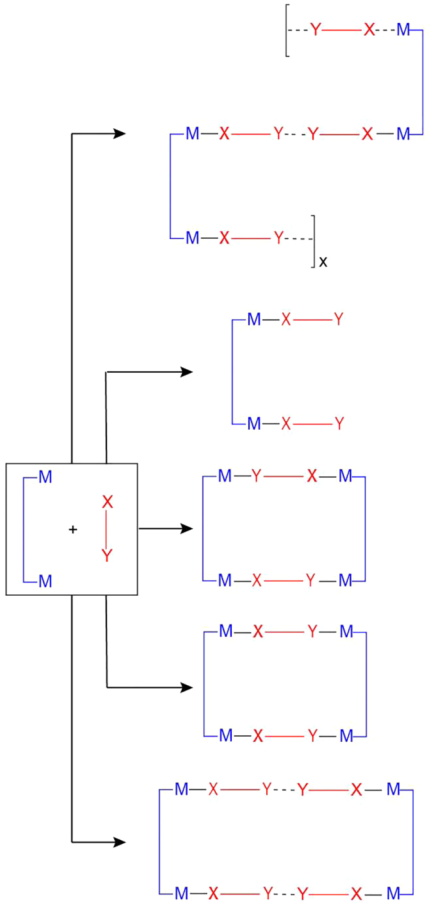

[a]Black dashed lines indicate a hydrogen-bond interaction, and solid black lines indicate a metal−ligand interaction.

Understanding the requirements for selective access to one product over another is important for understanding the possible applications of this new class of structures based on these hybrid MLHB ligand subunits.

RESULTS AND DISCUSSION

Synthesis of the 5-PYQ Hybrid MLHB Ligand. The pyridine-based MLHB ligand 5-pyridyl-1*H*-quinolin-2-one (**5-PYQ**) was synthesized in five steps from commercially available precursors (Figure 1a). Reaction of ethyl vinyl ether and oxalyl

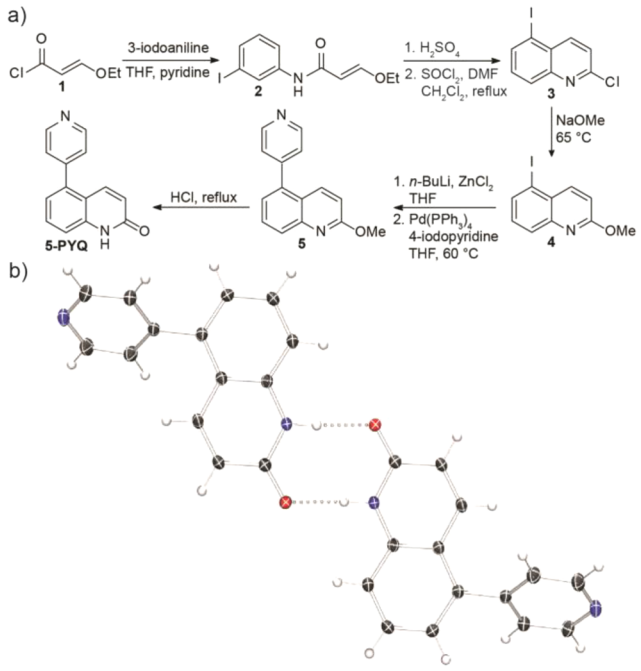

Figure 1. (a) Synthesis and (b) molecular structure of **5-PYQ**. Thermal ellipsoids in ORTEP diagram are shown at the 50% probability level.

chloride yields acid chloride **1**,[22] which is then used in the acylation of 3-iodoaniline to afford amide **2**. Cyclization of **2** with H_2SO_4, followed by reaction with $SOCl_2$ and purification by chromatography, yields 5-iodo-2-chloroquinoline (**3**). Subsequent protection with NaOMe generates 5-iodo-2-methyoxyquinoline (**4**), which was then coupled with 4-iodopyridine by reaction with *n*-BuLi, $ZnCl_2$, and $Pd(PPh_3)_2$ to generate methoxy-protected **5**. Deprotection with HCl regenerates the quinolone motif, affording **5-PYQ**. Single crystals of **5-PYQ** suitable for X-ray diffraction were grown from a DMSO solution of **5-PYQ** and confirmed its molecular structure. **5-PYQ** self-associates to form a 2-fold-symmetric, 180° hydrogen-bonded dimer, with a N−H···O hydrogen-bond distance of 2.7784(14) Å (Figure 1b). The N−*H* hydrogen atom was located from the residual electron density map and is consistent with the quinolone tautomeric form observed previously in similar ligand scaffolds.[13]

Assembly of 5-PYQ with Half-Clip 6 and Clip 7. To investigate the preorganization possible in this system, we deconstructed clip **7**[23] to half-clip **6**[24] to reduce the number of rotational degrees of freedom, thus simplifying the system to gain insights into the spectroscopic signals representative of final assembly formation (Scheme 3). Monoplatinated **6** was

Scheme 3. Structure of Half-Clip 6 and Clip 7

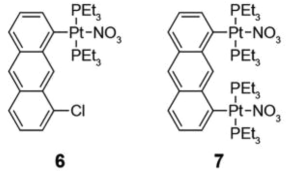

DOI: 10.1021/acs.inorgchem.5b00857
Inorg. Chem. 2015, 54, 6910−6916

treated with 2 equiv of **5-PYQ** with excess KPF_6 in a CH_2Cl_2/H_2O mixed solvent system; after stirring for 4 h at room temperature, the reaction mixture was washed with water and reduced in volume to afford half-rectangle **A** (Figure 2a).

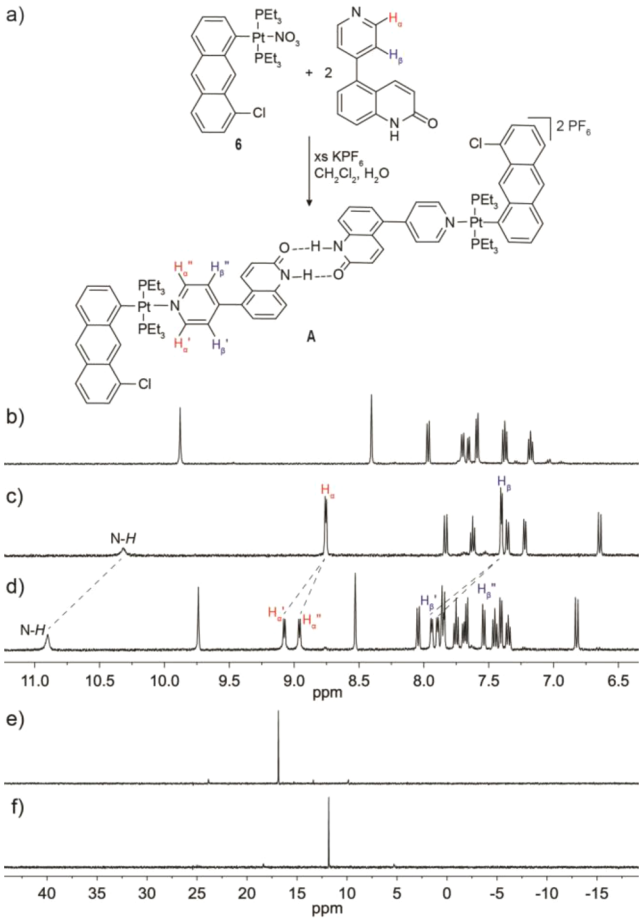

Figure 2. (a) Synthesis of half-rectangle **A**. (b) ^{1}H NMR spectrum (500 MHz, CD_2Cl_2) of half-clip **6**. (c) ^{1}H NMR spectrum (500 MHz, CD_2Cl_2) of **5-PYQ** with α-(red) and β-(blue) pyridyl proton signals colored for clarity. (d) ^{1}H NMR spectrum (500 MHz, CD_2Cl_2) for half-rectangle **A**, showing the downfield shift and splitting of the α-(red) and β-(blue) pyridyl protons upon **5-PYQ** binding Pt. (e) ^{31}P{^{1}H} NMR spectrum (202 MHz, CD_2Cl_2) of half-clip **6**. (f) ^{31}P{^{1}H} NMR spectrum (202 MHz, CD_2Cl_2) of half-rectangle **A**.

Analysis of the ^{1}H NMR spectrum of **A** suggested formation of a highly symmetric structure and provided distinct resonances from the monomeric **5-PYQ** and half-clip **6** subunits (Figure 2b–d). Particularly diagnostic were the downfield shifts of the α- and β-pyridyl proton signals of **5-PYQ** due to the loss of electron density upon platinum coordination. Coordination of the **5-PYQ** ligand to the platinum also results in restricted bond rotation, generating H'_α and H''_α, as well as H'_β and H''_β signals, which are also diagnostic of formation of the assembled structure (see Figure 2c and Figure 2d). Only one N–*H* resonance is observed in **A**, and it is shifted downfield from unbound **5-PYQ**, indicating that a symmetrical **5-PYQ** hydrogen-bonding environment is present in half-rectangle **A** (Figure 2c and Figure 2d). The ^{31}P{^{1}H} NMR spectrum of **A** also supports the formation of a single, highly symmetric species, as evidenced by the appearance of a sharp singlet at 11.82 ppm with ^{195}Pt satellites ($J_{P,Pt}$ = 2647.2 Hz) (Figure 2f). The new ^{31}P{^{1}H} NMR resonance for half-rectangle **A** is shifted 5.03 ppm upfield, relative to half clip **6**, which is again consistent with pyridyl binding Pt (Figure 2e,f).[23]

X-ray-quality crystals of half-rectangle **A** where grown by layering EtOH onto a CH_2Cl_2 solution of the assembly, which unambiguously confirmed the hydrogen-bonded structure of **A** (Figure 3). The crystal structure of half-rectangle **A** shows **5-PYQ** coordinated to the Pt center of half-clip **6** through the pyridine with a N–Pt length of 2.130(4) Å. The square planar geometry around the Pt center of half-clip **6** is maintained with an average N–Pt–P angle of 91.1°. The **5-PYQ** ligand maintains near-linear (173.0(6)°) hydrogen-bonded dimer character with an N–H···O bond distance of 2.777(6) Å. Table 1 summarizes bond lengths and angles for bonds of interest. Table 2 includes the crystallographic data for **5-PYQ** and half-rectangle **A**. The crystal packing of half-rectangle **A** contains π–π interactions (3.756 Å) of the anthracene rings of half-clip **6** and quinolone ring of **5-PYQ**. Interestingly, half-rectangle **A** appears to be preorganized in a geometry that would favor the formation of polymeric structures in the self-assembly of clip **7** and **5-PYQ**.

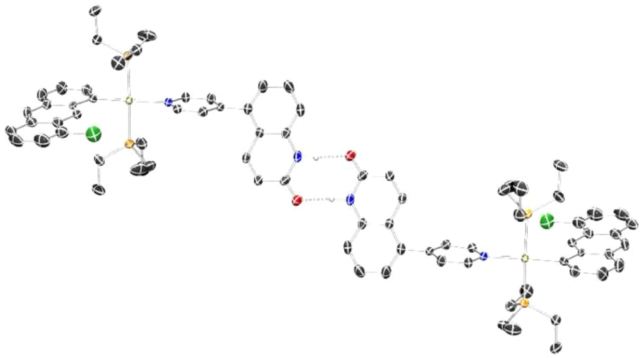

Figure 3. Molecular structure of half-rectangle **A**. Thermal ellipsoids in ORTEP diagram are shown at the 50% probability level.

Having established that the **5-PYQ** ligand can bridge two Pt centers while maintaining the quinolone hydrogen bonding, we used clip **7** to probe whether the **5-PYQ** ligand would yield one discrete species from a large number of potential self-assembled products. Such complexes include the coordination polymer (**B**), metal–ligand complex (**C**), macrocycle isomers (**D** and **E**) or hybrid MLHB rectangle (**F**) (see Scheme 4). Although the molecular structure of **A** is preorganized to favor the formation of a polymeric structure such as **B**, previous work with **7-DPQ** suggests that closed rectangle **F** could also be accessible. By contrast, if ambidentate metal–ligand interactions or inter-ligand π-stacking interactions are significant, coordination compounds **D** and **E** could also be accessed.

To determine which of the following structural arrangements were formed from full-clip **7**, we treated a CH_2Cl_2:H_2O solution of **7** with excess KPF_6 and 4 equiv of **5-PYQ** (Figure 4a). The resultant ^{1}H NMR spectrum of the crude reaction mixture showed peaks corresponding to a new compound, but also free **5-PYQ** ligand. Separation of these two species by chromatography yielded a product with a ^{1}H NMR spectrum consistent with macrocycle **D** (Figure 4a). Consistent with the restricted rotation of a pyridine ligand binding to clip **7**, two sets of doublets with downfield shifts were observed in the ^{1}H NMR spectrum for the α- and β-pyridyl protons (see Figure 4c and Figure 4d). Although we would expect a 2:1 pyridyl **5-PYQ**

DOI: 10.1021/acs.inorgchem.5b00857
Inorg. Chem. 2015, 54, 6910–6916

Table 1. Selected Bond Lengths and Angles of Half-Rectangle A

bond pair	bond/interaction length (Å)	bond angle	measurement (deg)
NH(1A)−O(2B)	2.777(6)	NH(1A)−O(2B)	173.0(6)
N(1A)−Pt(1A)	2.130(4)	N(1A)−Pt(1A)−P(1A)	90.52(12)
		N(1A)−Pt(1A)−P(2A)	91.78(12)
P(1A)−Pt(1A)	2.3041(14)	P(1A)−Pt(1A)−C(1A)	89.51(16)
P(2A)−Pt(1A)	2.3122(15)	P(2A)−Pt(1A)−C(1A)	88.08(16)
π(quin)−π(anth)	3.756	plane(quin)−plane(anth)	8.73

Table 2. Crystallographic Data for 5-PYQ and Half-Rectangle A

	5-PYQ	A
formula	$C_{14}H_{10}N_2O$	$C_{40}H_{48}ClF_6N_2OP_3Pt$
formula weight	222.24	1010.24
temperature (K)	100(2)	150(2)
crystal system	triclinic	monoclinic
space group	$P\bar{1}$	$P2_1/n$
a (Å)	7.7275(11)	9.5788(8)
b (Å)	8.7217(12)	16.5245(13)
c (Å)	8.9532(12)	25.198(2)
a (deg)	115.602(4)	90
b (deg)	74.194(3)	92.1140(15)
g (deg)	75.677(3)	90
V (Å^3)	535.09(13)	3985.8(6)
Z	2	4
r (mm^{-1})	1.379	1.684
m (mm^{-1})	0.089	3.771
F(000)	232	2016
crystal size (mm^3)	0.14 × 0.10 × 0.07	0.13 × 0.12 × 0.11
limiting indices	$-10 \le h \le 9$	$-11 \le h \le 11$
	$-11 \le k \le 11$	$-19 \le k \le 19$
	$-11 \le l \le 11$	$-29 \le l \le 29$
θ range (deg)	2.49−28.00	1.62−25.00
completeness to θ (%)	99.9	100.0
total reflections	10963	42411
independent reflections	2587	7986
data/restraints/parameters	2587/0/2194	7023/0/491
max, min transmission	0.9938, 0.9876	0.680, 0.650
$R1$ ($wR2$) [$I > 2\sigma(I)$]	0.0427 (0.1129)	0.0338 (0.0724)
$R1$ ($wR2$)	0.0517 (0.1195)	0.0517 (0.0811)
goodness of fit, GoF (F^2)	1.048	1.016
max, min peaks (e/Å^3)	0.422, −0.249	1.634, −1.037

Scheme 4. Self-Assembly of 5-PYQ with Clip 7 Selects Only for Macrocycle Isomer D, Rather than Polymer B, Metal-Ligand Complex C, Macrocyclic Isomer E, or Hybrid MLHB Rectangle F

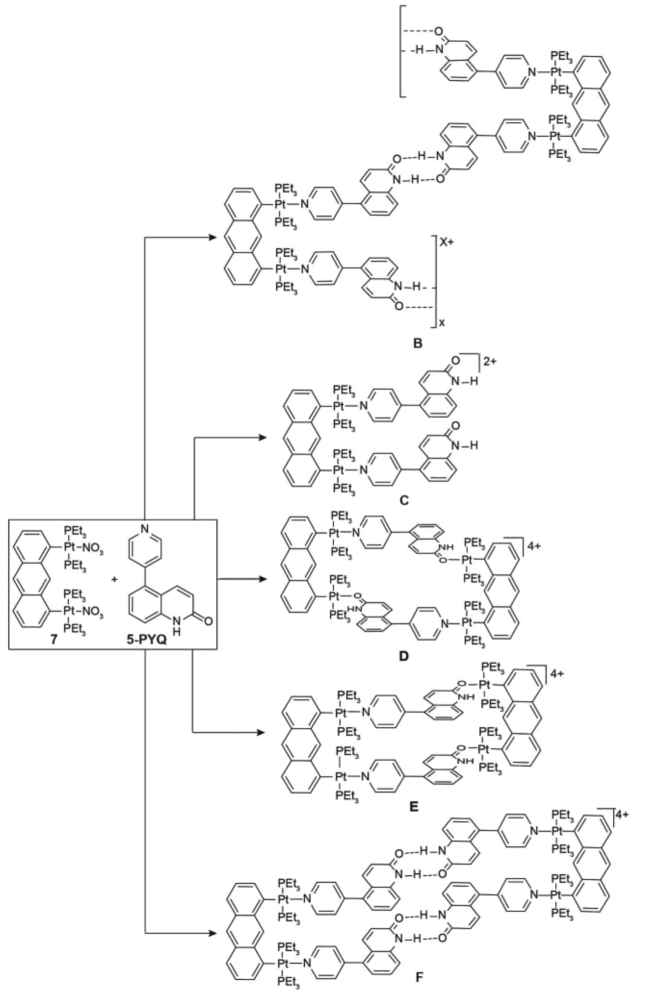

binding to **7** based on the structure of half-rectangle **A**, integrations suggest the presence of a complex with a 1:1 **5-PYQ**:**7** ratio, indicative of the formation of macrocycle isomers **D** or **E**. The $^{31}P\{^1H\}$ NMR spectrum of **D** displayed two sharp singlets at 8.89 ppm ($J_{P,Pt}$ = 2759.7 Hz) and 6.27 ppm ($J_{P,Pt}$ = 2725.1 Hz), shifted 4.48 and 7.10 ppm upfield relative to clip **7**, respectively, which is consistent with two different phosphorus environments as we would expect for macrocycle **D** or **E** (Figure 4d,f). The $^{31}P\{^1H\}$ NMR alone is not sufficient to distinguish whether macrocycle **D** or **E** is present. However, isomeric structures **D** and **E** can be differentiated by the anthracene H_9 and H_{10} resonances in the ^1H NMR spectrum. For example, isomer **E** would generate two sets of H_9 and H_{10} peaks, whereas isomer **D** would only generate one set of H_9 and H_{10} peaks, due to the presence of an inversion center at the center of the macrocycle. The ^1H NMR spectrum shows only one set of very sharp peaks for anthracene H_9 and H_{10} peaks, indicating macrocycle isomer **D** is the complex present in solution (Figure 4d). ^1H COSY and ^1H NOESY NMR experiments confirmed the ^1H NMR proton assignments discussed above. Furthermore, the ^1H NOESY NMR experiments reveal a strong NOE correlation of the **5-PYQ** N−*H* resonance and one set of PEt_3 groups, as well as a NOE signal of the **5-PYQ**−H_a and pyridyl−H_α protons, strongly indicating that macrocycle **D** is the complex found in solution (Figure 5). The NOE of pyridyl−H_α and all **5-PYQ** protons resonances indicate that there is a π-stacking interaction between the two Pt-bound **5-PYQ** ligands (Figure 5c, black circle), which may contribute to favoring the formation of the macrocycle **D** structure instead of the expected hybrid MLHB polymer (**B**) or rectangle (**F**).

DOI: 10.1021/acs.inorgchem.5b00857
Inorg. Chem. 2015, 54, 6910−6916

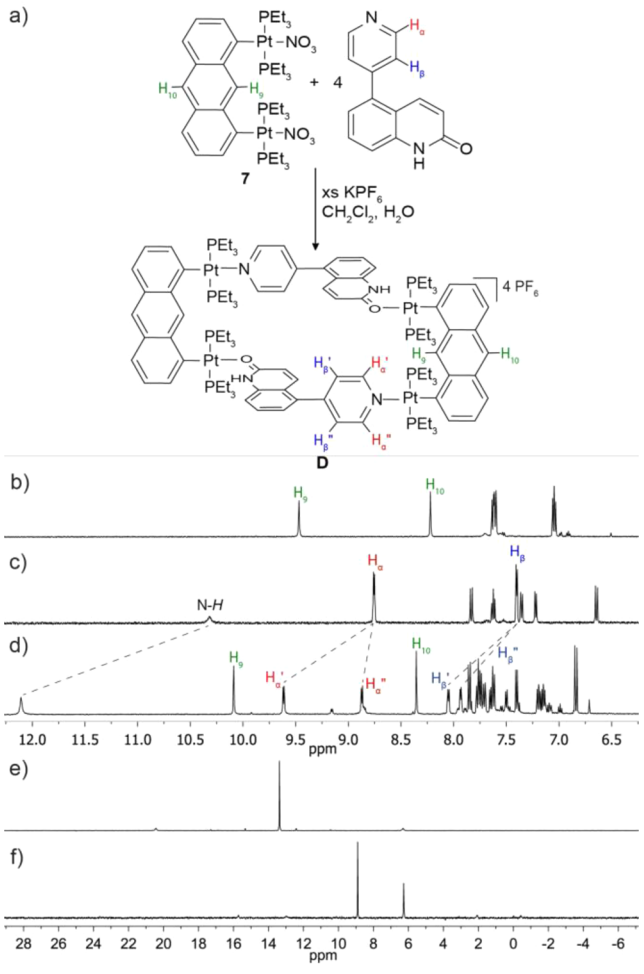

Figure 4. (a) Synthesis of macrocycle **D**. (b) ^{1}H NMR spectrum (500 MHz, CD_2Cl_2) of half-clip **6**. (c) ^{1}H NMR spectrum (500 MHz, CD_2Cl_2) of **5-PYQ** with α-(red) and β-(blue) pyridyl proton signals colored for clarity. (d) ^{1}H NMR spectrum (500 MHz, CD_2Cl_2) for macrocycle **D**, showing the downfield shift and splitting of the α-(red) and β-(blue) pyridyl protons upon **5-PYQ** binding Pt. (e) ^{31}P{^{1}H} NMR spectrum (202 MHz, CD_2Cl_2) of clip **7**. (f) ^{31}P{^{1}H} NMR spectrum (202 MHz, CD_2Cl_2) for macrocycle **D**.

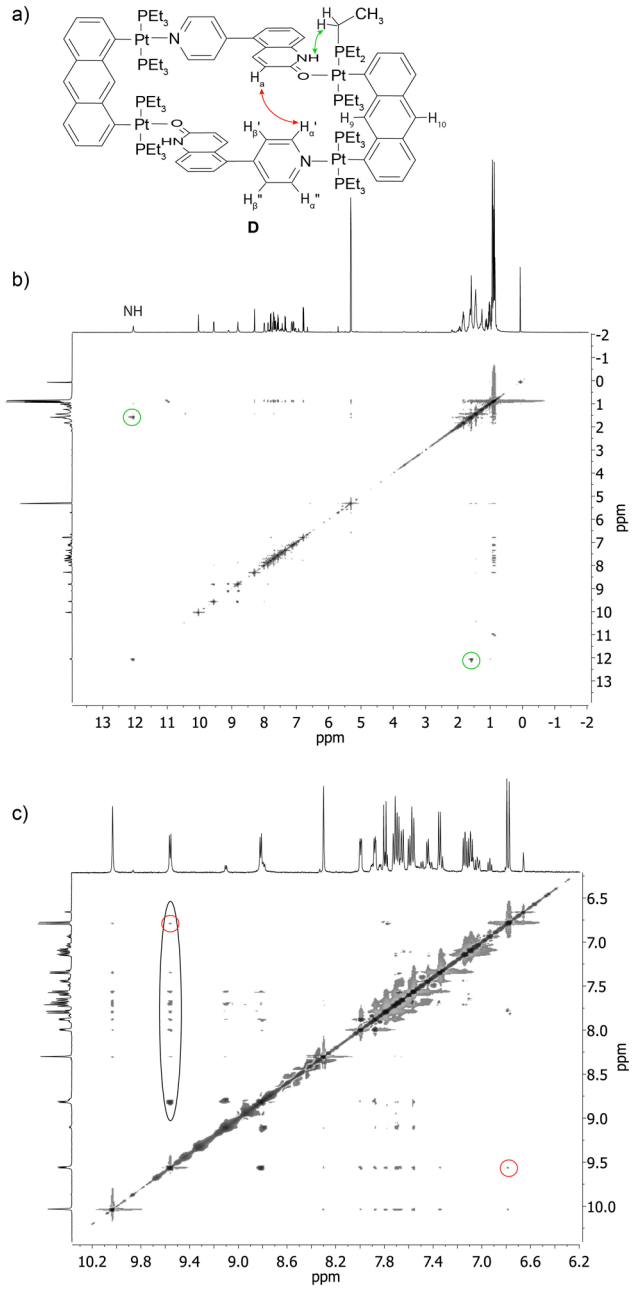

Figure 5. (a) Selected NOE contacts in macrocycle **D**, color coded to corresponding circled NOE signal for clarity. (b) ^{1}H NMR NOESY spectra (500 MHz, CD_2Cl_2) of macrocycle **D** and (c) zoom-in on aromatic region. The NOE between pyridyl–H_α and all of the **5-PYQ** protons is highlighted in black.

To further rule out formation of large polymeric structures like **B**, or oligomeric aggregates, we performed ^{1}H DOSY NMR experiments to investigate the diffusion coefficient of the reaction product and to determine whether multiple species were present in solution. ^{1}H DOSY NMR experiments confirmed the presence of one discrete species in solution, with a diffusion coefficient of $(4.45 \pm 0.05) \times 10^{-10}$ m^2 s^{-1} correlating to a radius consistent with the presence of the macrocycle **D** (see Figure 6). Table 3 compares the radii calculated from diffusion data with the crystallographic radii of **5-PYQ** and half-rectangle **A**. In both compounds, the solution and solid-state radii agree well, suggesting that the hydrogen-bonding remains intact in solution. The calculated radius of macrocycle **D** is consistent with the expected size (see Figure S18 for MMFF optimized structure), due to the more spherical nature of **D** by comparison to half-rectangle **A**.

CONCLUSION

In conclusion, we report the preparation of the pyridyl quinolone ligand **5-PYQ** and demonstrate that this ligand scaffold maintains self-complementary hydrogen bonding interactions when complexed with *mono*-platinated half-clip **6**. Upon treatment with *bis*-platinated **7**, a single discrete macrocycle is formed over other possible coordinate polymers, oligomers, or MLHB structures as evidenced by ^{1}H, ^{31}P{^{1}H}, NOESY, and DOSY NMR experiments. Selective macrocycle formation indicates that further investigation of this system could lead to potential applications in host–guest chemistry or catalysis. The selectivity for forming a single coordination macrocycle suggests that the interligand π-stacking interactions of **5-PYQ** outweigh the self-complementary quinolone hydrogen bonding interactions, providing new insights into the design requirements in self-assembled systems containing both metal–ligand and hydrogen-bonding interactions. Investigation

DOI: 10.1021/acs.inorgchem.5b00857
Inorg. Chem. 2015, 54, 6910–6916

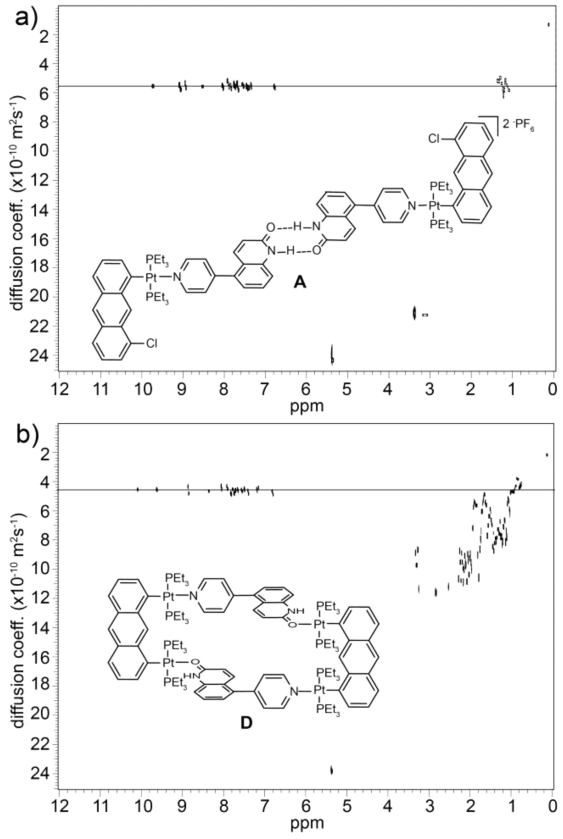

Figure 6. ^{1}H NMR DOSY spectra (500 MHz, CD_2Cl_2) of (a) half-rectangle **A** and (b) macrocycle **D**.

Table 3. Diffusion Data for 5-PYQ, Half-Rectangle A, and Macrocycle D, Including the Calculated Radii and Radii from the Determined Molecular Structures

	5-PYQ	half-rectangle **A**	macrocycle **D**
diffusion coefficient ($\times 10^{-10}$ m^2 s^{-1})	9.07 ± 0.56	4.98 ± 0.31	4.45 ± 0.23
radius (Å)			
Stokes–Einstein	5.87 ± 0.36	10.69 ± 0.35	11.04 ± 0.60
crystal structure[a]	5.98	10.12	

[a]Average of *x*, *y*, *z* radii.

of the quinolone interligand π-stacking interactions will be the focus of future studies and will be reported in forthcoming publications.

EXPERIMENTAL SECTION

Materials and Methods. All air- and moisture-sensitive reactions were performed under a nitrogen atmosphere using standard Schlenk and glovebox techniques. All chemicals were used as purchased unless noted otherwise. 3-Ethoxyprop-2-enoyl chloride (**1**),[22] 3-Ethoxy-*N*-(3-iodophenyl)acrylamide (2),[13] [1-*trans*-Pt$(PEt_3)_2NO_3$]-8-chloroanthracene (**6**),[24] and 1,8-bis(*trans*-Pt$(PEt_3)_2NO_3$)anthracene (**7**)[23] were prepared as previously described. Anhydrous and air-free solvents were obtained from a solvent purification system (Pure Process Technologies). Deuterated solvents were dried and deoxygenated by distillation over the appropriate drying agent followed by three freeze–pump–thaw cycles. NMR spectra were acquired on a Varian INOVA 500 MHz spectrometer at 25 °C and are referenced internally to residual protic solvent resonances. Data for ^{1}H, ^{31}P{^{1}H}, and ^{13}C{^{1}H} NMR spectra are reported as follows: chemical shift (δ, ppm), multiplicity: (s) singlet, (d) doublet, (t) triplet, (m) multiplet, integration, coupling constant (Hz). ^{1}H DOSY spectra were recorded using the PFG double stimulated echo pulse sequence. High-resolution mass spectrometry experiments were performed by the Biomolecular Mass Spectrometry Core of the Environmental Health Sciences Core Center at Oregon State University. Diffraction data were collected on a Bruker Smart Apex diffractometer at 150(2) K using Mo Kα radiation (λ = 0.71073 Å). Data reduction was performed in SAINT, and absorption corrections were applied using SADABS. All refinements were performed using the SHELXTL software package.[25−27] All non-hydrogen atoms were refined anisotropically. Hydrogen atoms were treated in calculated positions except those involved in hydrogen bonds, which were found on the residual density map and refined with isotropic thermal parameters.

*5-Iodo-2-chloroquinoline (**3**).* Solid **2** (5.76 g, 21.3 mmol) was added to concentrated H_2SO_4 (97%, 10 mL) and stirred at room temperature for 6 h. The resultant reaction mixture was poured into ice water (100 mL). The resultant precipitate was filtered, washed with Et_2O (25 mL), and dried to give a beige solid. The crude product (500 mg, 1.38 mmol) was dissolved in CH_2Cl_2 (30 mL) and $SOCl_2$ (130 μL, 214 μmol) and DMF (118 μL, 1.51 mmol) were added. The reaction mixture was refluxed for 3 h, cooled to room temperature, and poured into water (50 mL). After extraction with EtOAc (3 × 50 mL), the combined organic fractions were dried over $MgSO_4$, evaporated, and the residue was purified by flash chromatography (hexanes/EtOAc 9:1) to afford **3** (0.152 g, 28%) as white solid. ^{1}H NMR (500 MHz, CD_2Cl_2) δ: 8.40 (d, 1H, 8.8 Hz), 8.18 (d, 1H, 8.3 Hz), 8.03 (d, 1H, 8.3 Hz), 7.50 (m, 2H). ^{13}C{^{1}H} NMR (125 MHz, CD_2Cl_2) δ: 151.6, 148.0, 143.2, 138.2, 131.4, 129.5, 129.1, 123.9, 97.6. HRMS (*m*/*z*): [M +H]$^+$ calcd for C_9H_6NClI 289.9230, found 289.9092.

*5-Iodo-2-methyoxyquinoline (**4**).* A solution of **3** (0.651 g, 2.25 mmol) and NaOMe (10.1 mmol, prepared from 231.7 mg of Na in 10 mL of MeOH) was heated at 65 °C for 2 h. The reaction mixture was poured into a saturated aqueous NH_4Cl solution (10 mL) at 0 °C. After extraction with CH_2Cl_2, the combined organic layers were dried over $MgSO_4$ and evaporated to afford **4** (0.620 g, 97%) as a white solid. ^{1}H NMR (500 MHz, CD_2Cl_2) δ: 8.25 (d, 1H, 9.0 Hz), 7.98 (d, 1H, 7.6 Hz), 7.85 (d, 1H, 7.6 Hz), 7.35 (t, 1H, 7.6 Hz), 6.98 (d, 1H, 9.0 Hz), 4.10 (s, 3H). ^{13}C{^{1}H} NMR (125 MHz, CD_2Cl_2) δ: 163.6, 147.6, 143.3, 135.7, 131.0, 128.7, 127.6, 115.2, 98.4, 54.2. HRMS (*m*/*z*): [M+H]$^+$ calcd for $C_{10}H_9NOI$ 285.9729, found 285.9731.

*5-Pyridyl-2-methylquinoline (**5**).* In a glovebox, a solution of 4 (0.988 g, 3.46 mmol) in THF (30 mL) was cooled in a cold well cooled with liquid N_2, *n*-BuLi (2.73 mL of a 2.5 M solution in pentane, 6.93 mmol) was added slowly with stirring. The solution was allowed to sit in a cold well for 15 min, after which it was treated with a solution of $ZnCl_2$ (0.708 g, 5.19 mmol) in THF (10 mL). After an additional 15 min, a solution containing $Pd(PPh_3)_4$ (80 mg, 69 μmol) and 4-iodopyridine (1.42 g, 6.93 mmol) in THF (10 mL) was added to the reaction. The reaction mixture was then removed from glovebox, held on ice for 5 min, and then was heated to reflux under N_2 overnight. The solution was allowed to cool to room temperature and then cooled on an ice bath while H_2O (20 mL) was added. After extraction with CH_2Cl_2 (3 × 75 mL), the combined organic fractions were dried over $MgSO_4$, evaporated, and the residue was purified by flash chromatography (hexanes/EtOAc 3:2) to afford **6** (0.199 g, 24%) as white solid. ^{1}H NMR (500 MHz, CD_2Cl_2) δ: 8.75 (d, 2H, 5.4 Hz), 8.06 (d, 1H, 9.3 Hz), 7.94 (d, 1H, 8.8 Hz), 7.73 (t, 1H, 7.3 Hz), 7.44 (d, 2H, 5.9 Hz), 7.39 (d, 1H, 7.3 Hz), 6.93 (d, 1H, 9.3 Hz), 4.11 (s, 3H). ^{13}C{^{1}H} NMR (125 MHz, CD_2Cl_2) δ: 163.0, 150.4, 148.2, 147.6, 138.1, 136.6, 129.6, 128.4, 125.4, 125.3, 123.1, 113.9. HRMS (*m*/*z*): calcd for $C_{15}H_{13}N_2O$ 237.1028, found 237.1035.

*5-Pyridyl-1H-quinolin-2-one (**5-PYQ**).* Solid **6** (0.177 g, 0.749 mmol) was dissolved in concentrated HCl (5 mL) and refluxed for 6 h, after which the pH of the reaction mixture was adjusted to pH 7 with 6 M NaOH. The reaction mixture was extracted with a CH_2Cl_2/MeOH solution (3 × 20 mL), the organic fractions were combined and dried over $MgSO_4$, and the solvent was removed under reduced pressure to afford 5-PYQ as white solid (0.106 g, 64%). ^{1}H NMR (500 MHz, CD_2Cl_2/MeOD) δ: 8.68 (d, 2H, 5.4 Hz), 7.84 (d, 1H, 9.7 Hz), 7.631 (t, 1H, 7.33 Hz), 7.25 (m, 3H), 7.22 (d, 1H, 7.3 Hz), 6.63 (d, 1H, 9.7 Hz). ^{13}C{^{1}H} (125 MHz, CD_2Cl_2/MeOD) δ: 163.9, 149.8,

DOI: 10.1021/acs.inorgchem.5b00857
Inorg. Chem. 2015, 54, 6910−6916

148.2, 139.6, 138.7, 138.4, 131.1, 125.6, 124.2, 122.2, 117.8, 116.9. HRMS (m/z): calcd for dimer $C_{28}H_{21}N_4O_2$ 445.1665, found 445.1685.

*[1-(trans-Pt(PEt$_3$)$_2$(**5-PYQ**))-8-chloroanthracene]$_2$(PF$_6$)$_2$ (**A**).* KPF_6 (57.4 mg, 0.311 mmol) in water (1.5 mL) was added to a solution of anthPtCl (36.9 mg, 5.24 μmol) in CH_2Cl_2 (1.5 mL) and stirred vigorously for 20 min, after which a solution of **5-PYQ** (23.3 mg, 105 mmol) in CH_2Cl_2 (1.5 mL) and MeOH (0.5 mL) was added. The reaction mixture was then stirred vigorously for 4 h at room temperature. The organic layer was removed, washed with water (5 mL), and reduced to 1 mL under flow of N_2 and then layered with EtOH. Diffusion of EtOH into the saturated solution of CH_2Cl_2 afforded **A** as orange crystals (116 mg, 47%). ^{1}H NMR (500 MHz, CD_2Cl_2) δ: 10.89 (s, 1H), 9.73 (s, 1H), 9.07 (d, 1H, 5.8 Hz), 8.95 (d, 1H, 5.6 Hz), 8.52 (s, 1H), 8.04 (d, 1H, 8.5 Hz), 7.93 (d, 1H, 5.6 Hz), 7.89 (d, 1H, 5.6 Hz), 7.84 (m, 2H), 7.75 (t, 1H, 7.5 Hz), 7.68 (m, 2H), 7.53 (d, 1H, 7.8 Hz), 7.49 (t, 1H, 7.8 Hz), 7.40 (d, 1H, 7.3 Hz), 7.34 (t, 1H, 7.3 Hz), 6.82 (d, 1H, 10.0 Hz), 1.57−1.23 (m, 12 H), 1.14 (m, 18 H). ^{31}P{^{1}H} NMR (202 MHz, CD_2Cl_2) δ: 11.82 ppm ($J_{P,Pt}$ = 2647.1 Hz).

*[1,8-bis(trans-Pt(PEt$_3$)$_2$(**5-PYQ**))anthracene]$_2$(PF$_6$)$_4$ (**D**).* KPF_6 (30.4 mg, 165 μmol) in water (1.5 mL) was added to a solution of anthPt$_2$ (32.0 mg, 27.6 μmol) in CH_2Cl_2 (1.5 mL) and stirred vigorously for 20 min, after which a solution of **5-PYQ** (24.5 mg, 110 μmol) in CH_2Cl_2 (1.5 mL) and MeOH (0.5 mL) was added. The reaction mixture was stirred vigorously for 4 h at room temperature. The organic layer was removed, washed with water (5 mL), and evaporated to afford an orange-red solid that was purified by preparatory chromatography (5% MeOH:CH_2Cl_2) to afford **D** (42.2 mg, 49%) as a red-orange solid. ^{1}H NMR (500 MHz, CD_2Cl_2) δ: 12.05 (s, 1H), 10.03 (s, 1H), 9.56 (d, 1H, 5.3 Hz), 8.79 (d, 1H, 5.8 Hz), 8.29 (s, 1H), 7.99 (d, 1H, 4.6 Hz), 7.85 (d, 1H, 5.3 Hz), 7.76 (d, 1H, 9.7 Hz), 7.72−7.64 (m, 3H), 7.59 (d, 1H, 6.3 Hz), 7.49 (d, 1H, 8.3 Hz), 7.43 (d, 1H, 6.3 Hz), 7.34 (d, 1H, 7.3 Hz), 7.15−7.07 (m, 2H), 6.74 (d, 1H, 9.7 Hz), 1.83 (m, 12 H), 1.62 (m, 12 H), 1.46 (m, 12 H), 1.26 (m, 12 H), 1.04−0.84 (m, 72 H). ^{31}P{^{1}H} NMR (202 MHz, CD_2Cl_2) δ: 8.89 ppm ($J_{P,Pt}$ = 2759.79 Hz), 6.27 ppm ($J_{P,Pt}$ = 2725.1 Hz).

■ ASSOCIATED CONTENT

Ⓢ Supporting Information

Experimental details, NMR spectra, including DOSY, COSY, and NOESY experiments, MMFF optimized structure of **D**, and X-ray crystallographic data. The Supporting Information is available free of charge on the ACS Publications website at DOI: 10.1021/acs.inorgchem.5b00857.

■ AUTHOR INFORMATION

Corresponding Author

*E-mail: pluth@uoregon.edu.

Notes

The authors declare no competing financial interest.

■ ACKNOWLEDGMENTS

This work was supported by funding from the University of Oregon (UO). The NMR facilities at the UO are supported by the NSF/ARRA (Grant No. CHE-0923589). The Biomolecular Mass Spectrometry Core of the Environmental Health Sciences Core Center at Oregon State University is also acknowledged. Oregon State University is supported, in part, by the NIEHS (Grant P30ES000210) and the NIH.

■ REFERENCES

(1) Marshall, L. J.; de Mendoza, J. *Org. Lett.* **2013**, *15*, 1548−1551.
(2) Gianneschi, N. C.; Tiekink, E. R. T.; Rendina, L. M. *J. Am. Chem. Soc.* **2000**, *122*, 8474−8479.
(3) Burrows, A. D.; Mingos, D. M. P.; White, A. J. P.; Williams, D. J. *J. Chem. Soc., Dalton Trans.* **1996**, 3805−3812.
(4) Yamanaka, M.; Toyoda, N.; Kobayashi, K. *J. Am. Chem. Soc.* **2009**, *131*, 9880−9881.
(5) Yamanaka, M.; Kawaharada, M.; Nito, Y.; Takaya, H.; Kobayashi, K. *J. Am. Chem. Soc.* **2011**, *133*, 16650−16656.
(6) Sigel, R. K. O.; Freisinger, E.; Metzger, S.; Lippert, B. *J. Am. Chem. Soc.* **1998**, *120*, 12000−12007.
(7) Metzger, S.; Lippert, B. *J. Am. Chem. Soc.* **1996**, *118*, 12467−12468.
(8) Munakata, M.; Wu, L. P.; Yamamoto, M.; Kuroda-Sowa, T.; Maekawa, M. *J. Am. Chem. Soc.* **1996**, *118*, 3117−3124.
(9) Schnebeck, R. D.; Freisinger, E.; Glahe, F.; Lippert, B. *J. Am. Chem. Soc.* **2000**, *122*, 1381−1390.
(10) Young, M. C.; Liew, E.; Ashby, J.; McCoy, K. E.; Hooley, R. J. *Chem. Commun.* **2013**, *49*, 6331−6333.
(11) Young, M. C.; Holloway, L. R.; Johnson, A. M.; Hooley, R. J. *Angew. Chem., Int. Ed.* **2014**, 9832−9836.
(12) Piepenbrock, M. O. M.; Anderson, K. M.; Sansam, B. C. R.; Clarke, N.; Steed, J. W. *CrystEngComm* **2009**, *11*, 118−121.
(13) Sommer, S. K.; Zakharov, L. N.; Pluth, M. D. *Inorg. Chem.* **2015**, *54*, 1912−1918.
(14) Chakrabarty, R.; Mukherjee, P. S.; Stang, P. J. *Chem. Rev.* **2011**, 6810−6918.
(15) Northrop, B. H.; Zheng, Y. R.; Chi, K. W.; Stang, P. J. *Acc. Chem. Res.* **2009**, *42*, 1554−1563.
(16) Stang, P. J.; Olenyuk, B. *Acc. Chem. Res.* **1997**, *30*, 502−518.
(17) Seidel, S. R.; Stang, P. J. *Acc. Chem. Res.* **2002**, *35*, 972−983.
(18) Chi, K. W.; Addicott, C.; Arif, A. M.; Stang, P. J. *J. Am. Chem. Soc.* **2004**, *126*, 16569−16574.
(19) Mukherjee, P. S.; Das, N.; Kryschenko, Y. K.; Arif, A. M.; Stang, P. J. *J. Am. Chem. Soc.* **2004**, *126*, 2464−2473.
(20) Chatterjee, B.; Noveron, J. C.; Resendiz, M. J. E.; Liu, J.; Yamamoto, T.; Parker, D.; Cinke, M.; Nguyen, C. V.; Arif, A. M.; Stang, P. J. *J. Am. Chem. Soc.* **2004**, *126*, 10645−10656.
(21) Ghosh, S.; Mukherjee, P. S. *Dalton Trans.* **2007**, 2542−2546.
(22) Fernandez, F.; Garcia-Mera, X.; Morales, M.; Rodriguez-Borges, J. E. *Synthesis-Stuttgart* **2001**, 239−242.
(23) Kuehl, C. J.; Huang, S. D.; Stang, P. J. *J. Am. Chem. Soc.* **2001**, *123*, 9634−9641.
(24) Megyes, T.; Jude, H.; Grosz, T.; Bako, I.; Radnai, T.; Tarkanyi, G.; Palinkas, G.; Stang, P. J. *J. Am. Chem. Soc.* **2005**, *127*, 10731−10738.
(25) Sheldrick, G. M. *Acta Crystallogr., Sect. A: Found Crystallogr.* **2008**, *64*, 112.
(26) Sheldrick, G. M. *SHELXTL*; University of Göttingen: Göttingen, Germany, 2008.
(27) Sheldrick, G. M. *SHELXTL*; University of Göttingen: Göttingen, Germany, 2000.

DOI: 10.1021/acs.inorgchem.5b00857
Inorg. Chem. 2015, 54, 6910−6916